

Time-Varying Network Measures in Resting and Task States Using Graph Theoretical Analysis

Chia-Yen Yang¹ · Ching-Po Lin²

Received: 5 March 2014 / Accepted: 7 April 2015 / Published online: 16 April 2015
© Springer Science+Business Media New York 2015

Abstract Recent studies have shown the importance of graph theory in analyzing characteristic features of functional networks of the human brain. However, many of these explorations have focused on static patterns of a representative graph that describe the relatively long-term brain activity. Therefore, this study established and characterized functional networks based on the synchronization likelihood and graph theory. Quasidynamic graphs were constructed simply by dividing a long-term static graph into a sequence of subgraphs that each had a timescale of 1 s. Irregular changes were then used to investigate differences in human brain networks between resting and math-operation states using magnetoencephalography, which may provide insights into the functional substrates underlying logical reasoning. We found that graph properties could differ from brain frequency rhythms, with a higher frequency indicating a lower small-worldness, while changes in human brain state altered the functional networks into more-centralized and segregated distributions according to the task requirements. Time-varying connectivity maps could provide detailed information about the structure distribution. The frontal theta activity represents the essential foundation and may subsequently interact with high-frequency activity in cognitive processing.

Keywords Synchronization likelihood · Graph theory · Small worldness · Magnetoencephalography · Resting state · Task state

Introduction

Various techniques have been used in extensive studies of brain connectivity, which can be divided into structural, functional, and effective connectivities (Friston 2011). At the functional level there are two main methods for processing connectivity (van den Heuvel and Hulshoff Pol 2010). The first, most-straightforward method is to correlate the time series of a particular brain region with those of all other regions. In this approach the region of interest is typically called the seed, and the methods used to quantify linkages in a seed-based algorithm include correlation (Liu et al. 2010), covariance, mutual information (Ioannides 2001), and synchronization likelihood (SL) (a new measure for linear as well as nonlinear interdependencies between signals) (Montez et al. 2006; Stam et al. 2006; Olde Dubbelink et al. 2008; Bosboom et al. 2009a, b) in the time domain, and spectral coherence (Stam et al. 2006; Chang and Glover 2010), and phase locking (Lachaux et al. 1999) in the frequency domain. The second method does not employ a model and does away with the need to define a seed region a priori. In contrast to seed-based methods, this method looks for general patterns of connectivity across whole brain regions. Such approaches to seeking the co-existence of spatial sources include principal component analysis, independent component analysis (ICA) (De Luca et al. 2006), factor analysis, and hierarchical, Laplacian, and normalized cut clustering (Smit et al. 2010).

Interestingly, these biological networks are neither completely regular (e.g., a diffusively coupled system) nor

✉ Chia-Yen Yang
cyyang@mail.mcu.edu.tw

¹ Department of Biomedical Engineering, Ming-Chuan University, Taoyuan, Taiwan

² Brain Connectivity Laboratory, Institute of Neuroscience, National Yang-Ming University, Taipei, Taiwan

completely random, instead being called “small worlds” (Watts and Strogatz 1998). To represent the properties of neural networks, some recent studies have applied graph theoretical methods (Smit et al. 2008). This type of analysis represents a powerful tool for characterizing the topological organization of complex networks, and has recently been applied in studies of human brain networks related to both health and disease states (Tian et al. 2011). A small-world graph simply quantifies the structural properties based on characteristic path length L and clustering coefficient C (Watts and Strogatz 1998). In terms of information flow, a high clustering coefficient means that the nodes are strongly connected to one another (i.e., allowing modularized information processing functionally), and a short average shortest path length means that the network is more tightly integrated between nodes (i.e., allowing effective interactions or rapid transfer of information between regions) (Gong et al. 2009). For further quantifying connectivity profiles so as to provide a more-global description of the network, studies have investigated several complex network measurements, including the degree centrality (strength), shortest path length, clustering coefficient, betweenness centrality, closeness centrality, and eigenvector centrality (Rubinov and Sporns 2010). Since it was claimed that a small-world organization is a viable marker of genetic differences in human brain organization (Smit et al. 2008), the information of graph characteristics as well as in the excitability dynamics of cortical network should be important when looking for functional modules in human subjects exhibiting differences in cognition or behavior.

However, many studies have focused on extracting static graphs for describing relative long-term brain activity, which is not consistent with the well-known characteristic that all practical networks change over time both continuously and irregularly (Mutlu et al. 2012). Averaging these temporal series of graphs over an extended period of time represents a limitation of using static graphs in real-life applications that results in the loss of dynamic information (Moewes et al. 2013). Therefore, the present study aimed to establish and characterize functional networks based on SL and graph theory. For constructing quasidynamic graphs, a long-term static graph was simply divided into a sequence of subgraphs that each had a timescale of 1 s. The observed irregular changes were then used to explore differences in human brain networks between resting and specific activation states using the magnetoencephalography (MEG) technique, which may provide insights into the functional substrates underlying logical reasoning. Resting states form the essential basis of the brain for most of the ongoing cerebral energy consumption (Musso et al. 2010). Comparison with those activation-state processes based on certain resting states may provide

additional information about the underlying cognitive load, where seldom in the default states of brain function, and further for several neuropsychiatric disorders.

Methods

Subjects

Fourteen healthy males who were ophthalmologically and neurologically normal participated in this study. Their ages ranged from 25 to 32 years (28.5 ± 3.25 years, mean \pm SD). The visual acuity of all subjects was within the normal range (with correction, where necessary). Informed consents that had been approved by the local Ethics Committee of Yang-Ming University were obtained from all the participants.

Stimulation Procedure

Because responses in the eyes-open state differ from those in the eyes-closed state (which represents a more preparatory state for the former), the experiment for the resting state was divided into two conditions: relaxation with eyes closed and relaxation with eyes open. Subjects were instructed to minimize any movements and to try to think of nothing for 5 min but without falling asleep. In contrast, the experiment for the activation state involved a math-operation task. Eight math puzzles were used as stimulus material (see Fig. 1). The participants were instructed to provide their answers as accurately and rapidly as possible after the questions had been presented. Only the sections with the maximum proportions of correct answers were considered for further data analysis (among the 8 sections, 1 of them involving the maximum 12 subjects was analyzed in this study). These visual stimuli were generated in MATLAB (The MathWorks, Natick, MA) using functions provided by the Psychophysics Toolbox (Brainard 1997; Pelli 1997) on a personal computer, and projected onto a mirror by a projector. During the entire experiment the subject was positioned supine in a comfortable and stable position.

Data Acquisition

Neuromagnetic fields were recorded during the experiment with a whole-head 160-channel coaxial gradiometer (PQ1160C, Yokogawa Electric, Tokyo, Japan). The magnetic responses were filtered by a bandpass filter from 0.1 to 200 Hz and digitized at a sampling rate of 1200 Hz. For off-line analysis, the nonperiodic low-frequency noise in the MEG raw data was reduced using time-shift principal component analysis with three reference channels (de Cheveigné and Simon 2007). The resulting data were then

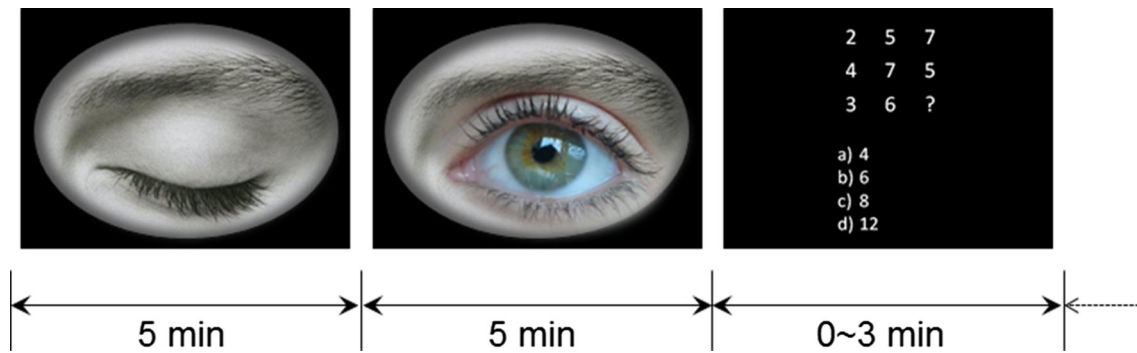


Fig. 1 Experimental design for the three tasks, showing the time course of serial stimulation. The dotted arrow indicates further stimuli that were presented in a random order

filtered by a simple 60-Hz Butterworth notch filter after removing artifacts with amplitudes exceeding 3000 fT/cm in the MEG signals. After the experimental procedures, the subject's head shape and position relative to the MEG sensor were measured using a three-dimensional digitizer and five markers.

Data Analysis

The exported MEG data were downsampled (to 600 Hz) and preprocessed to remove eye movements, blink artifacts, and electrocardiography activity by the FastICA algorithm (Hyvärinen et al. 2010). The cleaned data were then filtered into five frequency bands: delta (0.5–4 Hz), theta (4–8 Hz), alpha (8–12 Hz), beta (12–25 Hz), and gamma (25–45 Hz) bands; the first 1 s and the last 3 s of the original data in each section from all subjects were ignored to eliminate the possibility of attention transients associated with stimulus initiation and motor responses associated with finger movements, respectively, during task-state stimulation. The SL values between all combinations of the 157 included channels (which excluded the three reference channels) were calculated by an in-house program written in MATLAB. First, the SL parameters are determined in each frequency band as follows: The time-delay embedding theorem is used to form a state-space representation of the system dynamics. This step involves selecting the correct time lag, l , and the dimension of the embedding vector, m , in state space $X_i = (x_i; x_{i+l}; x_{i+2l}; x_{i+3l}; \dots; x_{i+(m-1)l})$. According to Montez et al. (2006), $l = f_s/3HF$ and $m = 3HF/LF + 1$ while $W_1 = 2l(m-1)$ and $W_2 = 10/p_{\text{ref}} + W_1$, where HF is the highest frequency, LF is the lowest frequency, and p_{ref} equaled 0.01 in this study. Second, a critical Euclidean distance is estimated for different time points: critical distance ε is defined as a difference between embedded vectors closer to each other at a fixed probability p_{ref} , which was chosen independently for each channel in this step according to

$$p_{\text{ref}} = \frac{1}{N} \sum_{j=1}^N \theta(\varepsilon_{X,i} - |X_i - X_j|) \\ = \frac{1}{N} \sum_{j=1}^N \theta(\varepsilon_{Y,i} - |Y_i - Y_j|),$$

where θ is the Heaviside step function whose value is 1 for a positive argument and 0 for a negative or zero argument, and N is the number of vectors. Third, the SL calculation is performed for different time points as follows: Recurrences in one system were sought between time points i and j with the threshold distance. This comparison reflects how close they have to be in order to be considered in a similar state. The SL between systems X and Y at time i was defined as (Stam and van Dijk 2002)

$$SL_i = \frac{n_{XY}}{(W_2 - W_1 + 1) \times p_{\text{ref}}},$$

where n_{XY} is the number of simultaneous repetitions in systems X and Y given by

$$n_{XY} = \sum_{j=i-W_2/2}^{i-W_1/2} n + \sum_{j=i+W_2/2}^{i+W_1/2} n, \\ n = \theta(\varepsilon_X - |X_i - X_j|) \theta(\varepsilon_Y - |Y_i - Y_j|).$$

The obtained SL values (which ranged between 0 and 1) for each subject and for each frequency band were formed into 157×157 symmetrical binary and weighted matrices, respectively (but not causally), using a threshold (the whole range of T values, $0.01 < T < 1$, with increments of 0.001) so as to keep the average number of edges per node ($K = 5$) similar (Tan et al. 2013) and using normalizing on the interval of $[0, 1]$ to avoid individual differences (Navas et al. 2013) under the three experimental conditions. The values obtained for each subject were then averaged over 1 s to form a series of connecting maps. Finally, graph theory was used to describe different network systems by reducing their essence with parameters (Smit et al. 2008; van Diessen et al. 2013) for different time points: for

binary networks we calculated the small worldness as $S = \frac{C/C_r}{L/L_r}$ (where C_r is the average cluster coefficient of 10 random graphs with the same number of nodes and edges, and L_r is the average shortest path length of 10 random graphs with the same number of nodes and edges) (Stam 2004); while for weighted networks we calculated the degree centrality (strength) as $D = \frac{1}{n} \sum_{i=1}^n \sum_{j \neq i}^n w_{ij}$ (where w_{ij} are the elements of weighted matrices and n is the number of nodes) (Barrat et al. 2004), the shortest path length as $L = \frac{1}{n} \sum_{i=1}^n \frac{1}{n-1} \sum_{j \neq i}^n \min\left\{\frac{1}{w_{ij}}\right\}$ (where $\min\{1/w_{ij}\}$ is the lowest sum of weights between nodes i and j) (Watts and Strogatz 1998), the betweenness centrality as $B = \frac{1}{n} \sum_{i=1}^n \frac{1}{(n-1)(n-2)} \sum_{j \neq i, k \neq i, j \neq k}^n \frac{n_{jk}}{g_{jk}}$ (where n_{jk} is the number of shortest paths between nodes j and k that pass through node i , and g_{jk} is the number of geodesic paths between nodes j and k) (Freeman 1979; Opsahl et al. 2010), the eigenvector centrality as $E = \frac{1}{n} \sum_{i=1}^n \frac{1}{\lambda} \sum_{j=1}^n w_{ij} v_j$ (where λ is the largest eigenvalue and v is the corresponding eigenvector) (Newman 2004), and the clustering coefficient as $C =$

$$\frac{1}{n} \sum_{i=1}^n \frac{\sum_{j \neq i} \sum_{k \neq (i,j)} w_{ij} w_{ik} w_{jk}}{\sum_{j \neq i} \sum_{k \neq (i,j)} w_{ij} w_{ik}} \quad (\text{Grindrod 2002; Stam et al. 2009}).$$

Statistical differences were analyzed by a one-way repeated-measures ANOVA (with Greenhouse–Geisser adjustment) with three levels (eyes-closed, eyes-open, and math-operation tasks) for brain waves in the five frequency bands. Bonferroni-corrected post hoc tests (paired t tests) were conducted only when significant main effects were detected ($p < 0.05$).

Results

Test Data Analysis

We applied procedures identical to those of Stam and van Dijk (2002) to verify the accuracy of our SL program. Two unidirectionally coupled Hénon systems (Schiff et al. 1996) were tested. In total, 4096 samples were simulated. Four tests were repeated ten times each, with the following parameters used in each analysis: $l = 1$, $m = 10$, $W_1 = 100$, $W_2 = 410$, and $p_{ref} = 0.05$. First, the relationship of SL between identical ($B_{id} = 0.3$) and nonidentical ($B_{id} = 0.1$) systems with various coupling strengths, ranging from 0 for uncoupled systems to 1 for complete coupling in steps of 0.1, was

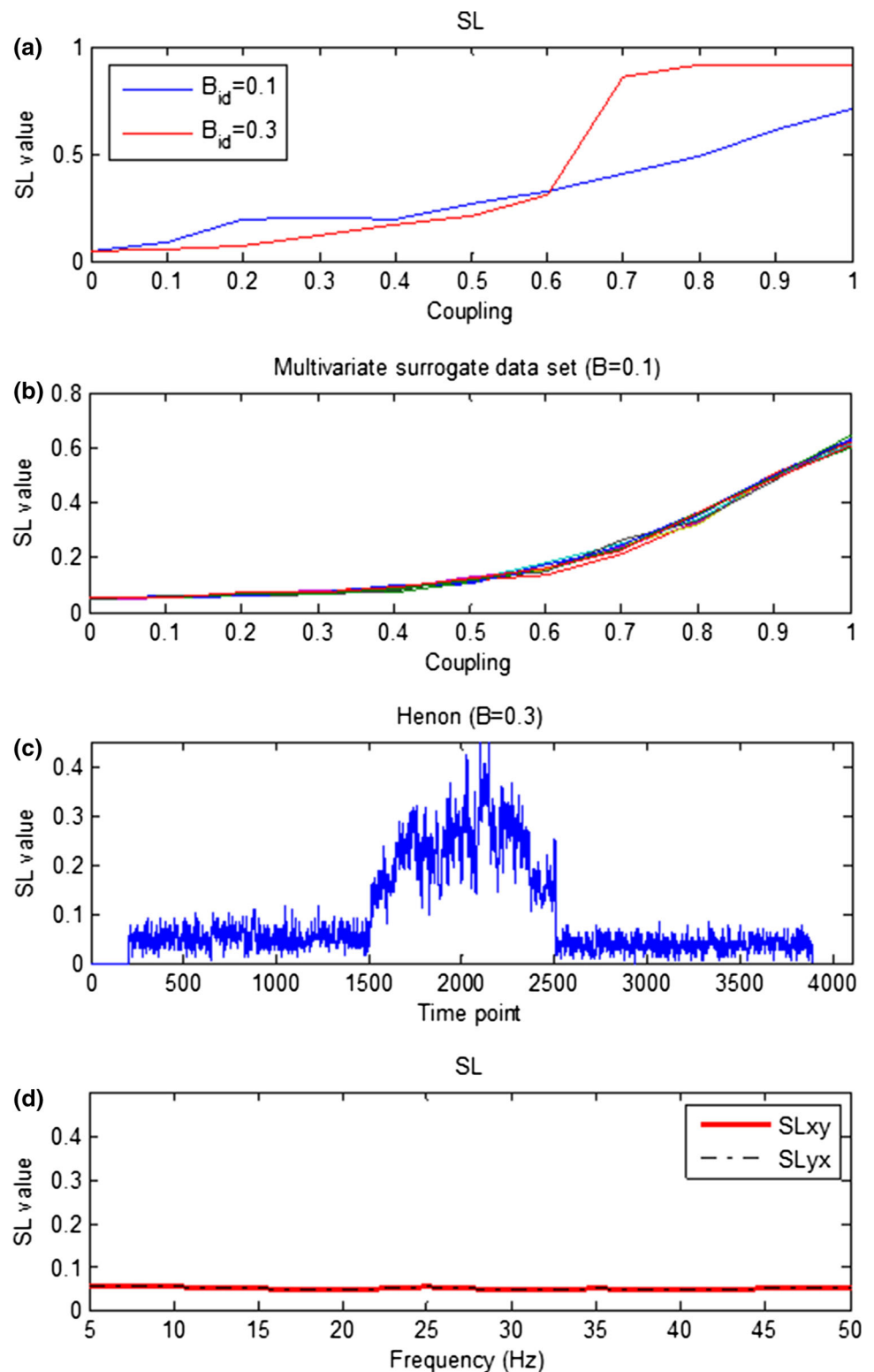
determined. The average results shown in Fig. 2(a) indicate that increasing the value of C_p increases SL both for the conditions. Second, the ability of SL to detect nonlinear coupling was determined by generating multivariate surrogate data in order to demonstrate that SL is sensitive to a nonlinear structure in the nonidentical coupling systems (Prichard and Theiler 1994). The average results shown in Fig. 2(b) indicate that SL increases with increasing C_p for the surrogate data. Third, the sensitivity of SL to time-dependent coupling strength was determined. The value of C_p was chosen to be 0 except in 1500–2500 samples; that is, $C_p = 0.5$ in the interval. The average results shown in Fig. 2(c) indicate the presence of a sharp increase in SL at 1500 samples and a sharp decrease at 2500 samples. Fourth, bias of SL in the estimates of dynamical interdependencies was determined. Random noise signals with and without low-pass filtering (from 5 to 50 Hz in steps of 5 Hz) were used to demonstrate that SL is not affected by the bias. The average results shown in Fig. 2(d) indicate that the SL does not depend upon the properties of the time series, and always fluctuates around 0.05, which is the value of p_{ref} in the test. Moreover, in order to verify the accuracy of our program in calculating parameters, we used the same simple graph example as used by Smit et al. (2008).

MEG Data Analysis

For binary networks, the MEG rhythms in each frequency band were used to calculate SL values and then construct functional connection maps with appropriate thresholds. Although the degrees in a map varied with time, the level was not obvious, in which cases grand degree K was represented as the probability distribution over the entire map. In the three tasks the values of grand degree K were varied from 2.05 to 14.98 as the threshold varied from 1 to 0.01, decreasing for all the frequency bands except the theta band (Table 1). K was largest for the delta and gamma bands when the threshold was 1 and 0.01, respectively. However, no significant difference was found in the delta, alpha, and gamma bands. The main effects of K values for tasks were significant ($p < 0.05$) in the theta band, which produced a positive shift to the math-operation situation compared to the other two situations. Thus, in order to compare different conditions further using graph theory, grand degree K was kept similar among the eyes-closed, eyes-open, and math-operation tasks.

Figure 3 shows parameters C/C_r and L/L_r (as graph properties at $K = 5$) calculated from the delta, theta, alpha, beta, and gamma activities of the 12 subjects for the eyes-closed, eyes-open, and math-operation conditions. No changes were apparent during the interval in each own task except in the delta band. Notably, the C/C_r values decreased (from approximately 4.2 to 1.2) as the frequency increased, whereas the L/L_r values remained at

Fig. 2 **a** Changes in SL as functions of C_p and B_{id} . **b** Changes in SL as a function of C_p in nonidentical unidirectionally coupled 10 multivariate surrogate data sets (shown with different colors). **c** Time dependence of SL in identical unidirectionally coupled Hénon systems. **d** Estimated interdependencies between two uncorrelated time series X and Y (Color figure online)



approximately 1.1. Also, the variation among subjects decreased as the frequency band increased. The ratio of C/C_r to L/L_r did not differ significantly with the experimental condition; however, the S values were all larger than 1 and decayed with frequency (Table 2).

For weighted networks, the MEG rhythms in each frequency band were used to calculate SL values and then construct functional connection maps with all of the obtained values. Figure 4 shows grand means of D , L , B , E , and C over the investigated time period calculated from the

Table 1 Grand degree K values (mean \pm SD) of binary networks constructed with minimum and maximum thresholds from the delta, theta, alpha, beta, and gamma activities of the 12 subjects over the

investigated time period among the eyes-closed, eyes-open, and math-operation tasks

Thres.	Freq. task	Delta	Theta	Alpha	Beta	Gamma
0.01	Eyes-closed	10.98 \pm 7.39	7.69 \pm 0.86	11.72 \pm 2.19	12.12 \pm 0.95	14.98 \pm 0.70
	Eyes-open	10.08 \pm 3.59	7.58 \pm 0.68	11.14 \pm 1.04	12.03 \pm 0.90	14.79 \pm 0.67
	Math-operation	9.92 \pm 2.34	8.28 \pm 1.31	10.96 \pm 1.37	12.38 \pm 1.96	14.88 \pm 0.64
1	Eyes-closed	8.43 \pm 4.91	2.25 \pm 0.06*	2.08 \pm 0.02	2.05 \pm 0.01	2.06 \pm 0.01
	Eyes-open	7.45 \pm 4.42	2.26 \pm 0.07**	2.08 \pm 0.02	2.06 \pm 0.01	2.07 \pm 0.02
	Math-operation	5.80 \pm 2.72	2.42 \pm 0.18*,**	2.08 \pm 0.03	2.07 \pm 0.06	2.06 \pm 0.01

*, ** significant difference ($p < 0.05$; one-way repeated-measures ANOVA with Greenhouse–Geisser adjustment and Bonferroni-corrected post hoc test)

delta, theta, alpha, beta, and gamma activities of the 12 subjects for the eyes-closed, eyes-open, and math-operation conditions. The main effects of the \bar{B} and \bar{C} values for tasks were significant ($p < 0.05$) in the theta band, which produced a negative shift in the eyes-open situation compared to the other two situations. In contrast, the \bar{D} , \bar{L} , and \bar{E} values did not differ significantly with the condition.

To look more closely at the connection maps in the bands of interest (i.e., theta, alpha, beta, and gamma), a stricter criterion (i.e., averaged values in the map greater than 0.1, indicating at least 10 % or 100 ms of the linkages existed during a 1-s period) was used in representative normalized series graphs changing with time (Fig. 5). The number of connections decreased slightly as the band frequency increased. C for the theta band differed significantly between the math-operation and the other two tasks. Apparent connections were found in the math-operation task in a cluster around the frontal area. E and C for the alpha and gamma bands, respectively, differed significantly between the math-operation and the other two tasks, producing a positive shift in the eyes-closed situation compared to the math-operation situation. Interestingly, the time point with significance changed from occurring early to late as the frequency increased.

Discussion

Test Data Analysis

The two coupled Hénon systems constitute a very simple test system, but four important simulation results were used to verify the validity of our program:

1. SL increases when the coupling strength between identical or nonidentical systems increases. Increasing C_p increases SL both for identical and nonidentical systems, though the relationship remains more

complex in the case of maximum coupling for nonidentical systems.

2. SL detects nonlinear coupling. With the test of two nonlinearly coupled chaotic systems, SL was shown to be able to detect the nonlinear coupling.
3. SL is sensitive to time-dependent changes in the coupling strength. The SL measure allows the detection of changes in coupling strength between systems as a function of time.
4. SL is insensitive to bias. Keeping the p_{ref} value fixed should allow SL to avoid the bias problem. This means that SL is not sensitive to any asymmetry in the coupling.

These four test results are identical to those reported by Stam and van Dijk (2002), which demonstrates the accuracy of our in-house program based on the concept of generalized synchronization for estimating dynamical interdependencies between time series.

Before using our method in a real-world application, a simple network graph was used to test the performance in examining small-world properties. All the values of parameters C and L were the same with those reported by Smit et al. (2008), which demonstrates the accuracy of our in-house program based on the concept of graph theory for estimating connective phenomenon in a network. A significant challenge would be expanding our technique to multichannel MEG data later.

MEG Data Analysis

All combinations of the 157 MEG channels provided a 157×157 matrix of SL values. For binary network analysis, a threshold to fix degree K was used to eliminate size and density effects of the graph network. According to van Wijk et al. (2010), a relatively large average degree for a network with a low overall connectivity may convert nonsignificant values into edges, whereas a relatively small one for a network with a high overall connectivity may neglect significant connections. Therefore, a series of

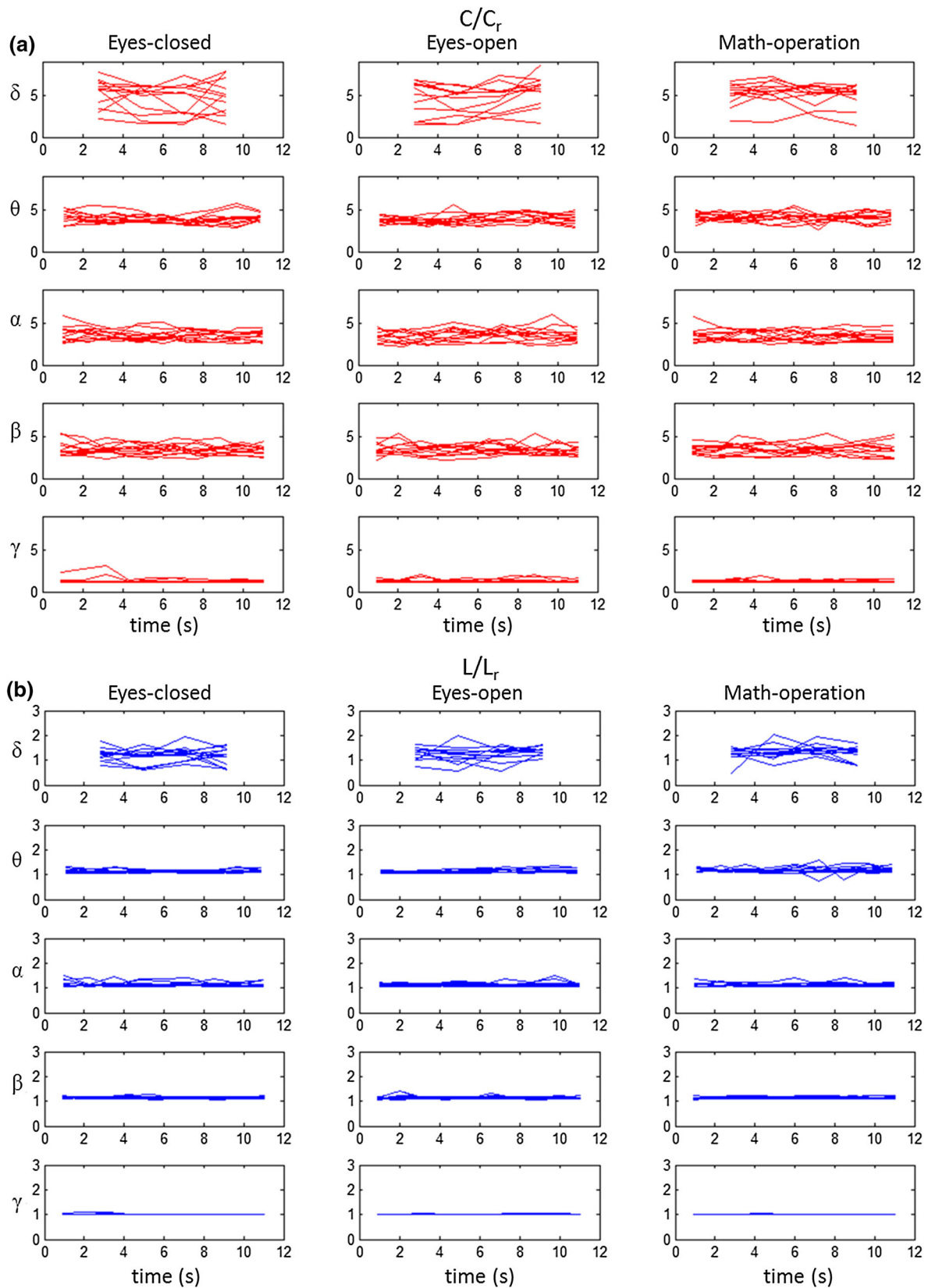


Fig. 3 Graph parameters C/C_r , **a** and L/L_r , **b** calculated at $K = 5$ from the delta, theta, alpha, beta, and gamma activities of the 12 subjects in the eyes-closed, eyes-open, and math-operation conditions

Table 2 Calculated values of S (mean \pm SD) at $K = 5$ binary networks from the delta, theta, alpha, beta, and gamma activities of the 12 subjects over the investigated time period among the eyes-closed, eyes-open, and math-operation tasks

Frequency	Task		
	Eyes-closed	Eyes-open	Math-operation
Delta	4.11 \pm 1.11	3.82 \pm 1.18	4.00 \pm 0.71
Theta	3.46 \pm 0.27	3.42 \pm 0.22	3.48 \pm 0.23
Alpha	3.09 \pm 0.29	3.07 \pm 0.38	3.05 \pm 0.34
Beta	3.02 \pm 0.43	2.99 \pm 0.42	3.04 \pm 0.50
Gamma	1.26 \pm 0.17	1.25 \pm 0.14	1.24 \pm 0.10

K values was first calculated with various thresholds in each condition for each subject, and then three selections for each frequency band were made to keep the grand degrees similar—and as close as possible to 5—in the eyes-closed, eyes-open, and math-operation tasks. This is based on the claim of Smit et al. (2008) that $K = 5$ seems to be the best representation of most of the variation shared between all levels of K .

To study the organization of functional connections in the brain, basic graph properties with a specific degree were used for comparing network topologies. Our results revealed that the C/C_r values varied with frequency within the range from 4.2 to 1.2, whereas the L/L_r values were maintained at

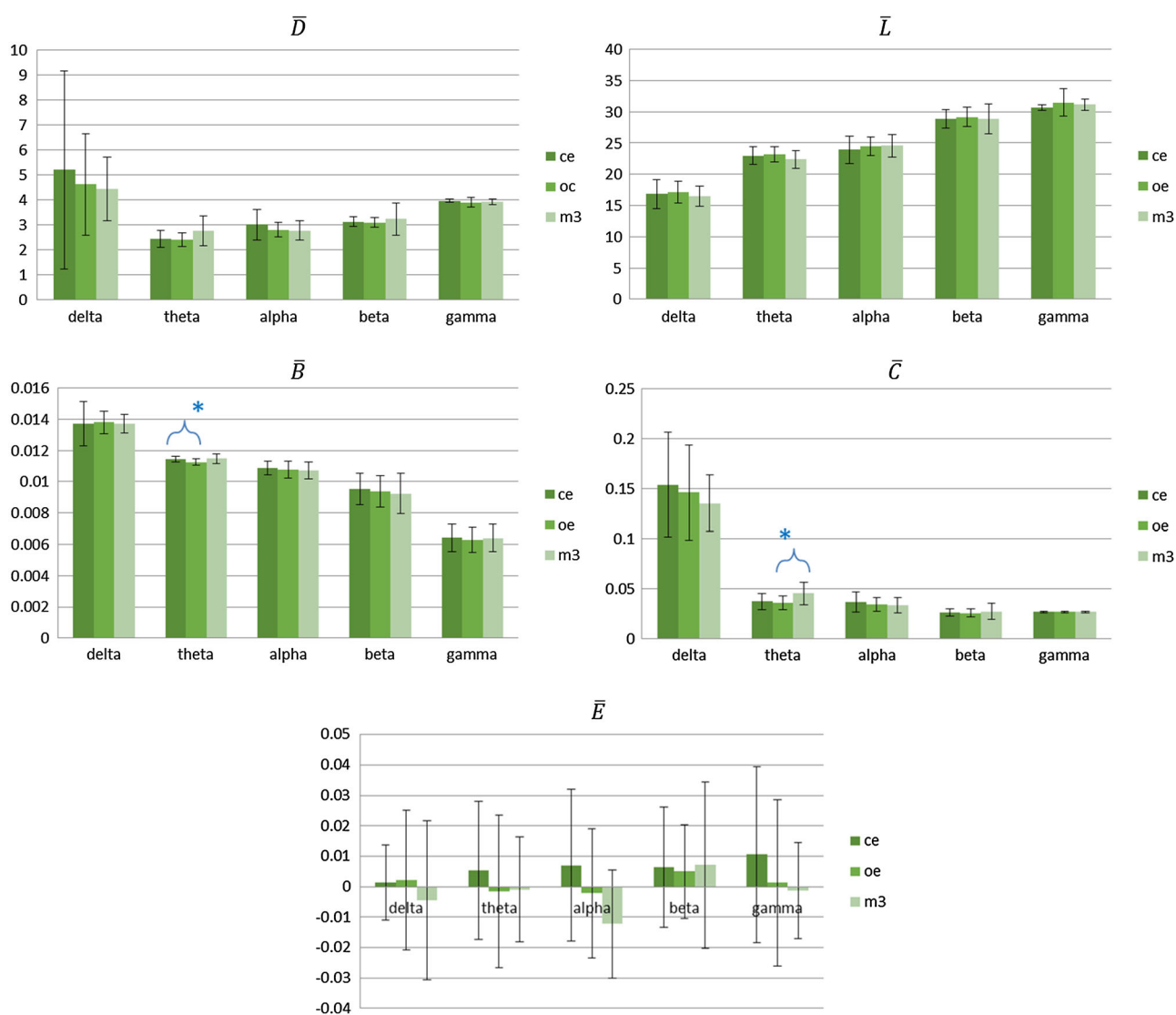


Fig. 4 Grand averages of parameters D , L , B , E , and C over the investigated time period calculated from the delta, theta, alpha, beta, and gamma activities of the 12 subjects for the eyes-closed (ce), eyes-open (oe), and math-operation (m3) conditions. Asterisks indicate

significance ($p < 0.05$) revealed by one-way repeated-measures ANOVA with Greenhouse–Geisser adjustment. Braces indicate significance ($p < 0.05$) revealed by Bonferroni-corrected post hoc test between two framed tasks

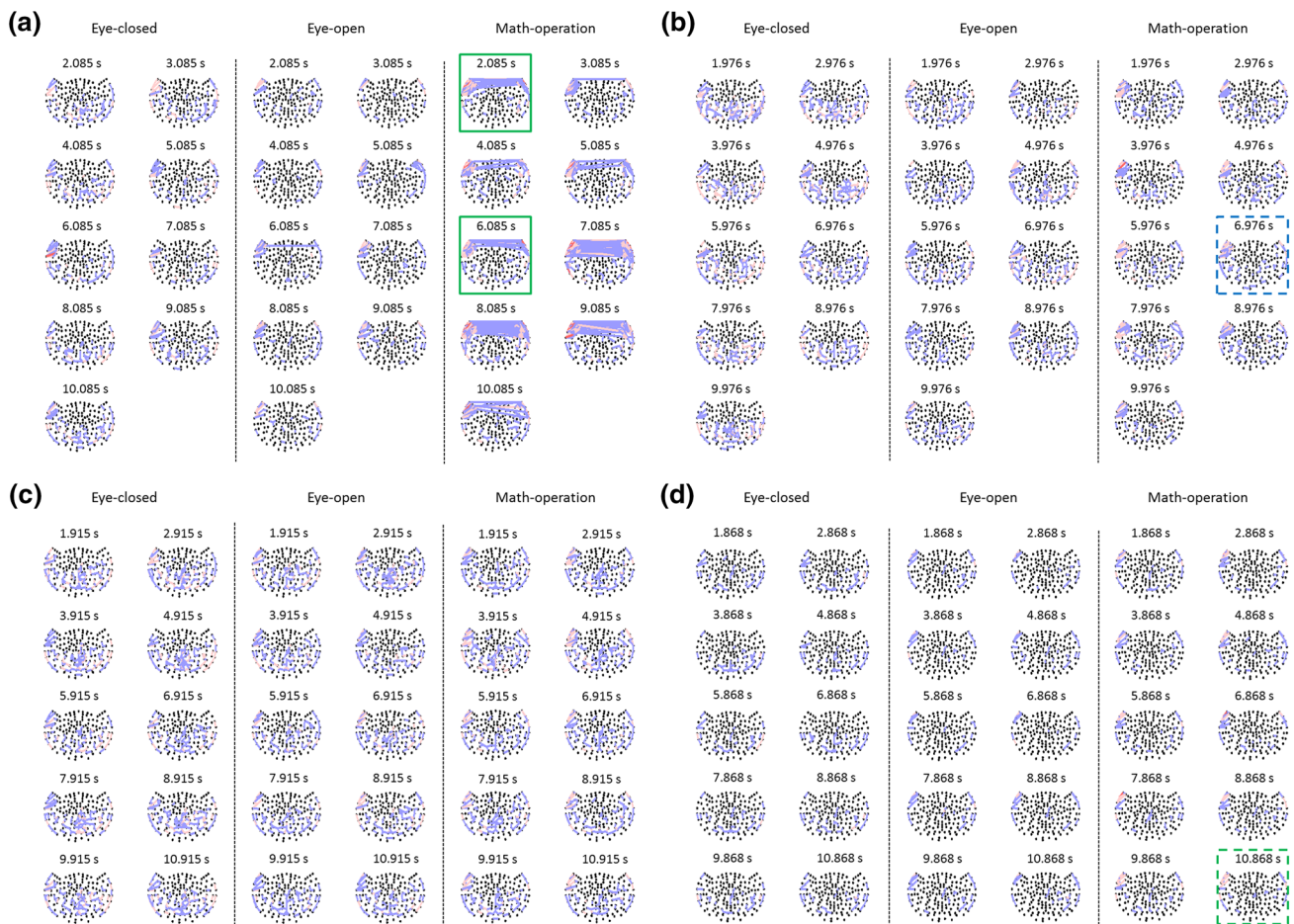


Fig. 5 Time-varying functional connection maps with 157 nodes for the theta (a), alpha (b), beta (c), and gamma (d) bands of 12 subjects among the 3 experimental conditions. Numbers indicate end time points. Colors from blue to red indicate averaged values during a 1-s period in the map from 0.1 to 1. Green and blue squares indicate

significant differences ($p < 0.05$) in C and E, respectively, between the math-operation and the eyes-closed tasks, with solid and dashed lines indicating higher and lower values, respectively (Color figure online)

approximately 1.1. This is consistent with the small-world model considered by Watts and Strogatz (1998) and echoes the reports of Smit et al. (2010), which used electroencephalography to examine the longitudinal genetic architecture of three parameters of functional brain connectivity, and of Douw et al. (2011), which claimed that better total cognitive performance was related to a higher clustering coefficient in the MEG delta and theta bands. Our statistical comparisons revealed that the values of small worldness S (i.e., the ratio between C/C_r and L/L_r) did not differ significantly between the eyes-closed and eyes-open tasks, although a prominent effect related to changes in thalamo-cortical and cortico-cortical synchronization should be expected during relaxed resting; that is, the alpha power being higher when the eyes are closed than when the eyes are open (Wu et al. 2010), and the ratio of mean cluster coefficients to mean shortest path lengths being larger when the eyes are closed than when the eyes are open (Tan et al. 2013). This may be explained by the concepts

in graph theory that describe the whole property but not the local distribution of the network. However, these S values did exhibit that tendency and were all larger than 1, especially in the low-frequency bands, as the small-world definition is based on a trade-off between high local clustering and short path length, which verified the small-world property of human brain networks. This is in indirect agreement with Wang et al. (2012), who conducted a functional MRI experiment to demonstrate that the brain functional organization maintained a robust, stable, and efficient small-world configuration during internal complicated information processing across task and resting states.

For weighted network analysis, five parameters were chosen to detect various aspects of functional integration, segregation, and centrality: First, the degree, D , of all nodes in the network is an important marker of network development and resilience, which describes the strength of network connections (Rubinov and Sporns 2010). Because D is a local

measure and does not account for correlations of link strength or specific distributions of the weights in the network (Navas et al. 2013), no significant variation in \bar{D} with the condition could be explained. Second, the shortest path length, L , corresponds to the ability to rapidly combine specialized information from distributed brain regions, since shorter paths imply a stronger potential for integration (Rubinov and Sporns 2010). Although \bar{L} did not differ significantly with the condition, the mean value in each condition increased from the low-frequency band to the high-frequency band. Jensen and Colgin (2007) showed cross-frequency interactions from the human neocortex, which suggested that slow oscillations serve to synchronize networks over long distances whereas fast oscillations are thought to synchronize cell assemblies over relatively short spatial scales. In that case the mean path from one node to every other node would require more steps when gamma-band activity is present. Third, the betweenness centrality B , is a more sensitive index that quantifies how much central nodes participate and consequently act as important controls of information flow. \bar{B} for the theta band differed significantly between the eyes-closed and eyes-open conditions, which suggests the existence of hubs but with a noisier distribution in the resting state (Navas et al. 2013). Fourth, the eigenvector centrality, E , is able to capture an aspect of centrality that extends to global features of the network with the greatest connectivity (Zuo et al. 2012). \bar{E} did not differ significantly with the condition, which may be due to the way we averaged all values, including positive and negative ones; this is not the most suitable measure for evaluating changes in network centrality. Fifth, clustering coefficient C corresponds to the ability for specialized processing to occur within densely interconnected groups of brain regions, with a large number of triangles implying segregation (Rubinov and Sporns 2010). \bar{C} for the theta band differed significantly between the math-operation and eyes-open conditions, which suggests that local information transmission is more efficient when performing a task and is in line with the economy theory of brain networks, which states that short-range system connections have lower costs (Achard and Bullmore 2007).

Differences in the theta, alpha, beta, and gamma bands prompted the drawing of SL maps in order to reveal the method of frequency processing under each condition. Linkages in the theta connectivity patterns at the frontal lobe were more concentrated during the math-operation task. Also, apparent network segregation could be found in this frequency band. Langer et al. (2013) revealed that the functional small-world topology of theta-band coherence varies between individuals as a function of working memory performance, especially in parietal and frontal regions, which implies that the spatial distribution of theta-band signals reflects the pattern of cognitive situations in an individual. Linkages in the

alpha connectivity patterns were dispersed, but centrality differed significantly only between the eyes-closed and math-operation tasks. By comparing eyes-open with eyes-closed resting states, Chen et al. (2013) found salient functional networks in the alpha band with a more distinct posterior than anterior focus. The difference in functional connectivity between two states reflects some intrinsic differences in information communication in the human brain (Tan et al. 2013). Linkages in the gamma connectivity patterns were dispersed, but at later times the segregation differed significantly between the eyes-closed and math-operation tasks. Many authors have discussed the involvement of activity at higher frequencies in several behavioral and pathological situations of arousal (e.g., Stoffers et al. 2008; Bosboom et al. 2009a, b; Schoonheim et al. 2013). The weak clustering in the gamma band relative to the theta band may reflect a specific coupling as a mechanism to transfer information from large-scale brain networks to the fast, local cortical processing required for effective computation and synaptic modification, thus integrating functional systems across multiple spatiotemporal scales (Jensen and Colgin 2007; Canolty and Knight 2010).

Conclusion

This study used SL and graph theory algorithms to quantify complex brain networks in different frequency bands. For binary network analysis, parameter S indicates that graph properties could differ with brain frequency rhythms, with higher frequencies have a lower small-worldness (i.e., decreasing local connectivity and increasing overall efficiency). For weighted network analysis, parameters B and C indicate that changes in human brain state altered the functional networks into more-centralized and segregated distributions according to task requirements. Time-varying connectivity maps could then provide detailed information about the structure distribution during eyes-closed, eyes-open, and math-operation tasks, where low frequencies represent the essential foundation and may subsequently interact with high-frequency activity during cognitive processing.

Acknowledgments This study was supported in part by research grants from National Science Council (NSC-101-2410-H-130-025-MY2, NSC 100-2628-E-010-002-MY3), Taiwan.

References

- Achard S, Bullmore E (2007) Efficiency and cost of economical brain functional networks. *PLoS Comput Biol* 3(2):e17
- Barrat A, Barthelemy M, Pastor-Satorras R, Vespignani A (2004) The architecture of complex weighted networks. *Proc Natl Acad Sci USA* 101(11):3747–3752

- Bosboom JL, Stoffers D, Stam CJ, Berendse HW, Wolters ECh (2009a) Cholinergic modulation of MEG resting-state oscillatory activity in Parkinson's disease related dementia. *Clin Neurophysiol* 120(5):910–915
- Bosboom JL, Stoffers D, Wolters ECh, Stam CJ, Berendse HW (2009b) MEG resting state functional connectivity in Parkinson's disease related dementia. *J Neural Transm* 116(2):193–202
- Brainard DH (1997) The psychophysics toolbox. *Spat Vis* 10(4):433–436
- Canolty RT, Knight RT (2010) The functional role of cross-frequency coupling. *Trends Cognitive Sci* 14(4):506–515
- Chang C, Glover GH (2010) Time-frequency dynamics of resting-state brain connectivity measured with fMRI. *Neuroimage* 50(1):81–98
- Chen JL, Ros T, Gruzelier JH (2013) Dynamic changes of ICA-derived EEG functional connectivity in the resting state. *Hum Brain Mapp* 34(4):852–868
- de Cheveigné A, Simon JZ (2007) Denoising based on time-shift PCA. *J Neurosci Methods* 165(2):297–305
- De Luca M, Beckmann CF, De Stefano N, Matthews PM, Smith SM (2006) fMRI resting state networks define distinct modes of long-distance interactions in the human brain. *Neuroimage* 29(4):1359–1367
- Douw L, Schoonheim MM, Landi D, van der Meer ML, Geurts JJ, Reijneveld JC et al (2011) Cognition is related to resting-state small-world network topology: an magnetoencephalographic study. *Neuroscience* 175:169–177
- Freeman LC (1979) Centrality in social networks. Conceptual clarification. *Soc Netw* 1(3):215–239
- Friston KJ (2011) Functional and effective connectivity: a review. *Brain Connectivity* 1(1):13–36
- Gong G, He Y, Concha L, Lebel C, Gross DW, Evans AC et al (2009) Mapping anatomical connectivity patterns of human cerebral cortex using in vivo diffusion tensor imaging tractography. *Cereb Cortex* 19(3):524–536
- Grindrod P (2002) Range-dependent random graphs and their application to modeling large small-world Proteome datasets. *Phys Rev E* 66(6 Pt 2):066702
- Hyvärinen A, Ramkumar P, Parkkonen L, Hari R (2010) Independent component analysis of short-time Fourier transforms for spontaneous EEG/MEG analysis. *Neuroimage* 49(1):257–271
- Ioannides AA (2001) Real time human brain function: observations and inferences from single trial analysis of magnetoencephalographic signals. *Clin Electroencephalogr* 32(3):98–111
- Jensen O, Colgin LL (2007) Cross-frequency coupling between neuronal oscillations. *Trends Cognitive Sci* 11(7):267–269
- Lachaux JP, Rodriguez E, Martinerie J, Varela FJ (1999) Measuring phase synchrony in brain signals. *Hum Brain Mapp* 8(4):194–208
- Langer N, von Bastian CC, Wirz H, Oberauer K, Jancke L (2013) The effects of working memory training on functional brain network efficiency. *Cortex* 49(9):2424–2438
- Liu Z, Fukunaga M, de Zwart JA, Duyn JH (2010) Large-scale spontaneous fluctuations and correlations in brain electrical activity observed with magnetoencephalography. *Neuroimage* 51(1):102–111
- Moewes C, Kruse R, Sabel BA (2013) Analysis of Dynamic Brain Networks Using VAR Models. In: Kruse R et al (eds) Synergies of soft computing and statistics for intelligent data analysis advances in intelligent systems and computing. Springer, Berlin, pp 525–532
- Montez T, Linkenkaer-Hansen KB, van Dijk W, Stam CJ (2006) Synchronization likelihood with explicit time-frequency priors. *Neuroimage* 33(4):1117–1125
- Musso F, Brinkmeyer J, Mobascher A, Warbrick T, Winterer G (2010) Spontaneous brain activity and EEG microstates. A novel EEG/fMRI analysis approach to explore resting-state networks. *Neuroimage* 52(4):1149–1161
- Mutlu AY, Bernat E, Aviyente S (2012) A signal-processing-based approach to time-varying graph analysis for dynamic brain network identification. *Comput Math Methods Med*. doi:10.1155/2012/451516
- Navas A, Papo D, Boccaletti S, del-Pozo F, Bajo R, Maestú F et al (2013) Functional hubs in mild cognitive impairment. *Int J Bifurc Chaos*. arXiv:1307.0969
- Newman ME (2004) Analysis of weighted networks. *Phys Rev E* 70(5 Pt 2):056131
- Olde Dubbelink KT, Felius A, Verbunt JP, van Dijk BW, Berendse HW, Stam CJ et al (2008) Increased resting-state functional connectivity in obese adolescents; a magnetoencephalographic pilot study. *PLoS One* 3(7):e2827
- Opsahl T, Agneessens F, Skvoretz J (2010) Node centrality in weighted networks: generalizing degree and shortest paths. *Soc Netw* 32(3):245–251
- Pelli DG (1997) The VideoToolbox software for visual psychophysics: transforming numbers into movies. *Spat Vis* 10(4):437–442
- Prichard J, Theiler D (1994) Generating surrogate data for time series with several simultaneously measured variables. *Phys Rev Lett* 73(7):951–954
- Rubinov M, Sporns O (2010) Complex network measures of brain connectivity: uses and interpretations. *Neuroimage* 52(3):1059–1069
- Schiff SJ, So P, Chang T, Burke RE, Sauer T (1996) Detecting dynamical interdependence and generalized synchrony through mutual prediction in a neural ensemble. *Phys Rev E* 54(6):6708–6724
- Schoonheim MM, Geurts JJ, Landi D, Douw L, van der Meer ML, Vrenken H et al (2013) Functional connectivity changes in multiple sclerosis patients: a graph analytical study of MEG resting state data. *Hum Brain Mapp* 34(1):52–61
- Smit DJ, Stam CJ, Posthuma D, Boomsma DI, de Geus EJ (2008) Heritability of “small-world” networks in the brain: a graph theoretical analysis of resting-state EEG functional connectivity. *Hum Brain Mapp* 29(12):1368–1378
- Smit DJ, Boersma M, van Beijsterveldt CE, Posthuma D, Boomsma DI, Stam CJ et al (2010) Endophenotypes in a dynamically connected brain. *Behav Genet* 40(2):167–177
- Stam CJ (2004) Functional connectivity patterns of human magnetoencephalographic recordings: a ‘small-world’ network? *Neurosci Lett* 355(1–2):25–28
- Stam CJ, van Dijk BW (2002) Synchronization likelihood: an unbiased measure of generalized synchronization in multivariate data sets. *Physica D* 163(3):236–251
- Stam CJ, Jones BF, Manshanden I, van Cappellen van Walsum AM, Montez T, Verbunt T et al (2006) Magnetoencephalographic evaluation of resting-state functional connectivity in Alzheimer's disease. *Neuroimage* 32(3):1335–1344
- Stam CJ, de Haan W, Daffertshofer A, Jones BF, Manshanden I, van Walsum AMVC et al (2009) Graph theoretical analysis of magnetoencephalographic functional connectivity in Alzheimer's disease. *Brain* 132(Pt 1):213–224
- Stoffers D, Bosboom JL, Deijen JB, Wolters ECh, Stam CJ, Berendse HW (2008) Increased cortico-cortical functional connectivity in early-stage Parkinson's disease: an MEG study. *Neuroimage* 41(2):212–222
- Tan B, Kong X, Yang P, Jin Z, Li L (2013) The difference of brain functional connectivity between eyes-closed and eyes-open using graph theoretical analysis. *Comput Math Methods Med*. doi:10.1155/2013/976365
- Tian L, Wang J, Yan C, He Y (2011) Hemisphere- and gender-related differences in small-world brain networks: a resting-state functional MRI study. *Neuroimage* 54(1):191–202

- van den Heuvel MP, Hulshoff Pol HE (2010) Exploring the brain network: a review on resting-state fMRI functional connectivity. *Eur Neuropsychopharmacol* 20(8):519–534
- van Diessen E, Otte WM, Braun KP, Stam CJ, Jansen FE (2013) Improved diagnosis in children with partial epilepsy using a multivariable prediction model based on EEG network characteristics. *PLoS One* 8(4):e59764
- van Wijk BC, Stam CJ, Daffertshofer A (2010) Daffertshofer, Comparing brain networks of different size and connectivity density using graph theory. *PLoS One* 5(10):e13701
- Wang Z, Liu J, Zhong N, Qin Y, Zhou H, Li K (2012) Changes in the brain intrinsic organization in both on-task state and post-task resting state. *Neuroimage* 62(1):394–407
- Watts DJ, Strogatz SH (1998) Collective dynamics of ‘small-world’ networks. *Nature* 393(6684):440–442
- Wu L, Eichele T, Calhoun VD (2010) Reactivity of hemodynamic responses and functional connectivity to different states of alpha synchrony: a concurrent EEG-fMRI study. *Neuroimage* 52(4):1252–1260
- Zuo XN, Ehmke R, Mennes M, Imperati D, Castellanos FX, Sporns O et al (2012) Network centrality in the human functional connectome. *Cereb Cortex* 22(8):1862–1875